Optics and Lasers in Engineering 161 (2023) 107401

Contents lists available at ScienceDirect

Optics and Lasers in Engineering

journal homepage: www.elsevier.com/locate/optlaseng

Review

Error analysis and compensation method of displacement measurements based on reflection projection imaging

Hai Yu*, Qiuhua Wan, Lihui Liang, Yingcai Du, Xinran Lu

Changchun Institute of Optics, Fine Mechanics and Physics, Chinese Academy of Sciences, Changchun 130033, People's Republic of China

ARTICLE INFO

Keywords:
Displacement measurement
Reflection projection imaging
Light wave intensity model
Measurement error

ABSTRACT

Displacement measurement technology based on an image recognition method can realize high-performance more easily than traditional technology. Compared with a transmission-type displacement measurement method illuminated by parallel light, a method based on reflection projection recognition can achieve smaller volume and have great advantages in an application environment with limited volume. However, due to the spherical light-field effects of point light used in reflection-type displacement measurement, the illumination intensity in different areas of an image sensor is different, resulting in some displacement measurement errors. Therefore, this study analyzed displacement measurement error based on reflective projection imaging and presented a corresponding error compensation method. First, taking the point light as the emission source, a miniaturized displacement measurement mechanism was proposed based on reflection projection imaging. Then, according to the wavefront recording model of the point light, a model of measurement error caused by differing illumination intensity was established. Finally, the corresponding compensation method was proposed and verified by simulations and experiments. After simulation analysis, the influencing factors of reflection-type displacement measurement error were established. When a circular grating with 86 mm diameter was used in experiments, the error compensation function proposed improved the measurement accuracy from 7.03 arcsec to 5.4 arcsec. Research done in this study demonstrated the error influencing factors of the reflective-type displacement measurement method and proposed an effective error compensation method, which thus laid a foundation for miniaturization and high-precision reflective-type displacement measurement technology.

1. Introduction

Digital displacement measurement technology is the core feedback of numerical control machining equipment and its measurement performance directly affects the level of high-precision manufacturing technology. At present, the existing digital displacement measurement technologies mainly include optical grating, magnetic grating, capacitance grating, and time grating with various measurement methods well applied in the industrial field. In the research of capacitive grating, Anandan [1] proposed in 2017 a wide-range capacitive sensor for linear and angular displacement measurement. Yu [2] proposed in 2019 a high-precision absolute angular-displacement capacitive sensor using three-stage time-grating in conjunction with a remodulation scheme. In the study of time grating, Chen [3] proposed in 2015 a long range time-grating sensor for displacement measurement and achieved nanometer accuracy in his experiments. In the study of magnetic gratings, Park [4] and Nguyen [5] in 2021 carried out the research of high-precision magnetic grating. Meanwhile, optical grating displacement measurement technology has been widely used because of its strong anti-interference feature, simple structure, and ability to easily perform large-range measurements. In 2020, Ye [6,7] proposed an electronic interpolator based on the ratio metric linearization conversion method and a precise phase demodulation algorithm and achieved high measurement resolution and accuracy.

Among above measurement methods, optical grating measurement technology has been widely used in various fields because of its high measurement accuracy, strong anti-interference, and ease in realizing large range measurement. In optical grating displacement measurement technology, how to achieve higher measurement resolution and higher measurement accuracy in a small size range has become a research hotspot.

Traditional optical grating displacement measurement technology mainly depends on "Moiré fringe" or other spatial measurement signals [8]. According to previous research, the traditional photoelectric displacement measurement method has the following shortcomings: 1) In order to achieve higher measurement resolution, the traditional method needs to rely on higher density scribed lines. Restricted by the optical diffraction limit, crosstalk between code channels, and other factors, higher density scribed lines cannot be further realized on small-size

* Corresponding author.
E-mail address: yuhai@ciomp.ac.cn (H. Yu).

https://doi.org/10.1016/j.optlaseng.2022.107401
Received 13 June 2022; Accepted 18 November 2022
Available online 25 November 2022

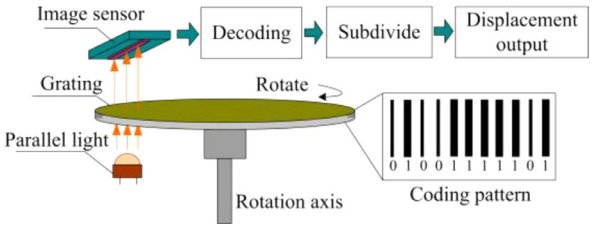

Fig. 1. Transmission-type IDM method.

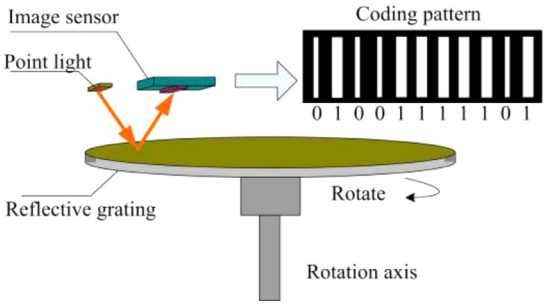

Fig. 2. Principle of reflection-type IDM.

grating disks. 2) If the traditional measurement method wants to realize absolute measurement, it needs to adopt mutual cooperation between the "coding track" and "incremental track." This leads to steps of "alignment period" and "staggering phase" between the signals of different code channels. A slight offset will cause measurement error. 3) The measurement accuracy of traditional measurement methods depends on the "ideal degree of Moiré fringe." If the measurement signal has changes such as "amplitude offset" and "phase offset," the measurement accuracy will decrease.

To solve the shortcomings of traditional measurement technology, image-type displacement measurement (IDM) technology has been proposed based on an image recognition method in previous research (Fig. 1) [9].

IDM technology uses digital image processing to recognize the preset pattern on the grating disk and then realizes high-resolution displacement measurements through a subpixel positioning algorithm. Based on the advantages of digital image processing, IDM has higher robustness, higher fault tolerance, and higher flexibility. Therefore, it has become a research hotspot for new high-performance optical grating displacement measurement technology.

According to the literature, in recent years, there have been several studies on IDM. Das [10] proposed in 2013 a displacement measurement method based on a gray gradient pattern, realizing a measurement resolution of 1 mm. Bajić [11] proposed in 2014 a displacement measurement method based on color recognition, which uses a disk coated with a uniform changing color to realize a rotation angle measurement with a linear error of 1°. Tomasz [12] proposed in 2015 a sequence coding method based on two-dimensional (2D) image recognition, which realizes $2^{n^{\wedge}2}$ position coding on *n*-circle code channels. Fu [13] proposed in 2015 a method for constructing a time-grating double coordinate system based on CCD pixels and realized ±2μm measurement accuracy. Mu [14] used in 2019 a CMOS image sensor to recognize single code channel pseudo-random code and realized 20-bit code recognition. Yuan [15] proposed in 2019 a high-precision subdivision algorithm with robust performance and achieved a measurement accuracy of 1.6 arcsec on a 79mm diameter grating disk. In 2020, Kim [16] has proposed a 2D plane displacement measurement coding method based on RGB three-channel color coding, which achieved a resolution of 0.5 μm and a maximum measurement error of 3.1 μm in the range of a 24 × 24 mm plane. Synthesizing the previous research progress, reducing the volume of the measuring device, and improving its accuracy is the research hotspot of many scholars.

In previous research, the author proposed an IDM method based on a linear image recognition method. The principle is to irradiate the transmission-type grating disk with a parallel light, map the pattern on the grating disk to the linear image sensor, and then realize the measurement and output of the current absolute displacement through a digital image processing algorithm. On this basis, in-depth research has been performed on methods for improving measurement resolution [17,18], methods for improving measurement accuracy [19,20] and methods for improving stain resistance [21]. Through previous research, it has been found that the transmission-type IDM method could further reduce the longitudinal height.

In this study, a reflection-type IDM method was proposed, using a point light to irradiate the grating disk. This realized the displacement measurement through the recognition of the reflection projection of the grating disk. Because the light wave emitted by the point light was a spherical light wave, there would be some measurement errors or even wrong output. Therefore, this paper analyzed the factors affecting the measurement and put forward an error compensation method for improving the measurement accuracy of reflection-type IDM, thus ensuring that measurement output was correct.

The main layout of this paper was: Section 2 presented the IDM principle based on reflection projection imaging. Section 3 established the error model and presented the error compensation method. Section 4 analyzed the proposed error model by simulation and pointed influencing factors. Section 5 was experimental verification and Conclusions presented in Section 6.

2. Reflection-type IDM

2.1. Measuring optical path

IDM technology mainly uses a linear image sensor to collect the pattern on a grating disk and then realizes high-performance displacement measurements through a digital-image processing algorithm. In the measurement light path of the previous study, the image sensor needs to be illuminated by a parallel light to realize transmission-type image acquisition [9]. Limited by the height of parallel light, the transmission-type measurement light path cannot further reduce the volume. Therefore, a reflection-type IDM optical path was proposed here (Fig. 2).

The system included a linear image sensor, point light, grating disk, and rotation axis. "Coded lines" for displacement measurement were drawn on the grating disk. When light emitted by the point light shined on the grating disk reflecting surface, the pattern of coded lines was reflected to the linear image sensor. The image sensor collected the gray value of the reflection projection and obtained the IDM value of the current position through subsequent calculation.

2.2. Decoding method

To realize displacement measurements, 2^N coded lines were drawn on the grating disk. All coded lines were located in a same diameter and all distances between adjacent coded lines the same. There were two kinds of coded lines in the circumference. The "wider" line was set to represent coding element "1" and the "narrower" line coding element "0". Through pseudo-random shift coding, single channel absolute coding was realized. When the number of coded lines in the circumference was 2^N, *N*-bit coding was formed in the circumference of the circular grating, as shown in the coding pattern in Fig. 2. At this time, the image collected by the linear image sensor needed to contain at least *N* coded lines. Adjacent *N*-coded lines formed a unique coding group. When the grating disk moved one position of the coded line, the coding group collected by the linear image sensor shifted once, so as to form a new

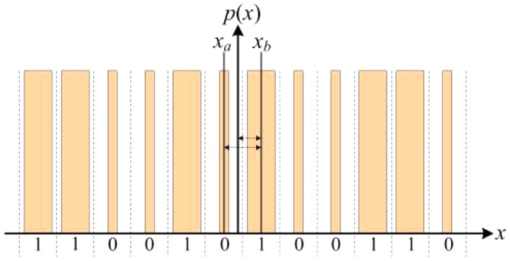

Fig. 3. Pattern collected by linear image sensor, including 12 lines.

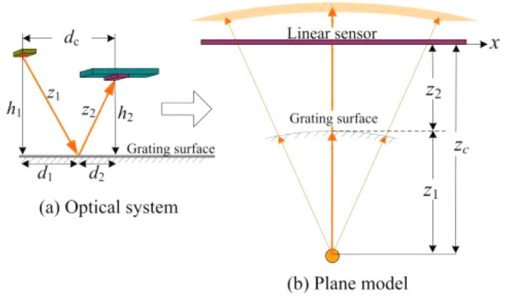

Fig. 4. Point light illumination model.

coding group. Each group of coding corresponded to a unique decoding value.

Through identification of the code, after the current coding group was obtained, the decoding value corresponding to the coding group was obtained by accessing a table and the decoding value set as value A.

2.3. Displacement subdivision principle

The measurement resolution was further improved by performing a "subdivision operation" between adjacent coded lines. The line pattern of a certain acquisition is shown in Fig. 3.

The coordinate system was established with the position of each pixel as the abscissa-axis, with the pixel gray value $p(x)$ as the vertical-axis, with the center point of the image as the zero point (Fig. 3). Examining the gray value information of 12 coded lines according to width, the 12 coded lines could be distinguished and the coding elements represented by them were (grouped in consecutive trios) {1, 1, 0, 0, 1, 0, 0, 1, 1, 0, 0, 1, 1, 0}. At the same time, the centroid positions of two coded lines on both sides of the coordinate origin were calculated by the centroid algorithm, which was expressed as x_a and x_b, respectively. The stability and accuracy of the centroid location algorithm was increased using a square weighted centroid algorithm for calculations, using Eq. 1, expressed as

$$x_a(x_b) = \frac{\sum_x x \cdot p(x)^2}{\sum_x p(x)^2} \tag{1}$$

where x limits to the range of each coded line pixel, from which the positioning points of two lines were calculated. Then, a ratio algorithm was used to calculate the subdivision value using Eq. 2, as

$$B = \eta \cdot \frac{x_b}{x_b - x_a} \tag{2}$$

where η is the subdivision multiple, which represents the numerical mapping of the spacing between adjacent coded lines. The larger the η was, the higher the resolution of measurement subdivision $\boldsymbol{B}$. However, due to the influence of factors, such as pixel gray value and noise in practical application, a too large η cannot be realized and its value needs to be determined by experiment.

Finally, after obtaining the decoding value $\boldsymbol{A}$ and subdivision value $\boldsymbol{B}$ at the same time, the final output of displacement measurement was expressed in Eq. 3, as

$$D = A \cdot \eta + B \tag{3}$$

3. Error analysis of reflection-type measurement

3.1. Light wave propagation function

According to the optical path in Fig. 2, the reflective optical path of the light wave emitted by the point light is shown in Fig. 4.

The spherical light wave emitted by the point light reached the linear image sensor after being reflected by the grating surface (Fig. 4a). In practical application, the height of the point light from the grating was h_1, the height of the linear image sensor from the grating h_2, and the lateral distance between the point light and linear image sensor $d_c = d_1 + d_2$. Then, d_1 and d_2 were represented in Eq. 4, as

$$\begin{cases} d_1 = \frac{d_c h_1}{h_1 + h_2} \\ d_2 = \frac{d_c h_2}{h_1 + h_2} \end{cases} \tag{4}$$

With the minimum optical distance from the point light to the grating as z_1 and the optical distance from the grating to the linear image sensor center z_2, then z_1 and z_2 was calculated using Eq. 5, expressed as

$$\begin{cases} z_1 = \sqrt{h_1^2 + d_1^2} \\ z_1 = \sqrt{h_2^2 + d_2^2} \end{cases} \tag{5}$$

For ease of analysis, the light wave model illuminated by the point light was changed into a plane model (Fig. 4b). The coordinate system was established with the straight line of the pixel on the linear image sensor as the x-axis and the center point of the linear image sensor as the origin. At this time, the light propagation distance between the point light and linear image sensor center was $z_c = z_1 + z_2$. Therefore, the optical distance from the point light to any position of the linear sensor was shown in Eq. 6, expressed as

$$r = \sqrt{z_c^2 + x^2} \tag{6}$$

As the light wave emitted from the point light was a spherical wave, the radius of the spherical wave was r in Eq. 6. For analytical convenience, the initial light field amplitude of the point light was assumed to be "u_0." Then, according to the light wave diffraction transfer function, the expression of the light field reaching the linear image sensor was expressed in Eq. 7, as

$$U(x) = \frac{u_0}{r} \exp\left[j\frac{2\pi r}{\lambda}\right] \tag{7}$$

where, $j = \sqrt{-1}$, λ is the wavelength of light wave, and the light field intensity $|U(x)|^2 = (u_0/r)^2$. As the linear image sensor only obtained the light intensity of the light field when collecting light, the distance between the pixel position and sensor center was let to be x and the collected pixel gray value directly proportional to the light field intensity, expressed in Eq. 8 as

$$p(x) = k \cdot |U(x)|^2 = k \cdot \frac{u_0^2}{z_c^2 + x^2} \tag{8}$$

where, k is a ratio coefficient between gray value and illumination intensity, which is a constant. Due to the change in transmission distance, the illumination intensity of the spherical light was different at the linear image sensor.

3.2. Error model

Affected by changes in light intensity, the gray value at different pixel positions on the linear image sensor also changed accordingly.

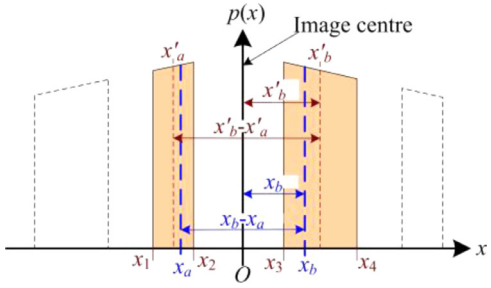

Fig. 5. Gray value curve of coded lines.

From the model Eq. 8, the gray value curves of two coded lines on both sides of the center point of the image sensor are shown in Fig. 5.

The upper end of a collected coded line was distorted due to the change in light wave irradiation intensity (Fig. 5). At this time, when the centroid algorithm in Eq. 1 was used for calculation, there was an offset.

When the coded line's range on the x-axis on the left side of the coordinate origin was set as $\{x_1–x_2\}$, then the gray values at positions x_1 and x_2 were expressed as Eq. 9 (Fig. 5), being

$$\begin{cases} p(x_1) = k \cdot \frac{u_0^2}{x_1^2+z_c^2} \\ p(x_2) = k \cdot \frac{u_0^2}{x_2^2+z_c^2} \end{cases} \tag{9}$$

When distortion existed, the gray value curve of every coded line was assumed to be approximately a "trapezoid." Therefore, according to the centroid algorithm, the centroid position of x'_a on the left side of the coordinate origin was shown in Eq. 10, as

$$\begin{aligned} x'_a &= \frac{\left[p(x_1)^2 \cdot x_1 + p(x_2)^2 \cdot x_2\right] \cdot (x_2 - x_1)/2}{\left[p(x_1)^2 + p(x_2)^2\right] \cdot (x_2 - x_1)/2} \\ &= \frac{x_1 \cdot \left(x_2^2+z_c^2\right)^2 + x_2 \cdot \left(x_1^2+z_c^2\right)^2}{\left(x_1^2+z_c^2\right)^2 + \left(x_2^2+z_c^2\right)^2} \end{aligned} \tag{10}$$

Similarly, corresponding to the coded line on the right side of the coordinate origin, the centroid position of x'_b was shown in Eq. 11, as

$$\begin{aligned} x'_b &= \frac{\left[p(x_3)^2 \cdot x_3 + p(x_4)^2 \cdot x_4\right] \cdot (x_4 - x_3)/2}{\left[p(x_1)^2 + p(x_2)^2\right] \cdot (x_4 - x_3)/2} \\ &= \frac{x_3 \cdot \left(x_4^2+z_c^2\right)^2 + x_4 \cdot \left(x_3^2+z_c^2\right)^2}{\left(x_3^2+z_c^2\right)^2 + \left(x_4^2+z_c^2\right)^2} \end{aligned} \tag{11}$$

Next, the situation when there was no light distortion was analyzed. The gray value curve of the coded line was assumed to be approximately a "rectangle," when there was no distortion. Then, the centroid positioning points were $x_a = (x_1+x_2)/2$ and $x_b = (x_3+x_4)/2$. Therefore, when the point light irradiated unevenly, the offsets from x_a and x_b were respectively shown in Eqs. 12 and 13.

$$\begin{aligned} \Delta a &= x_a - x'_a \\ &= \frac{(x_1+x_2)}{2} - \frac{x_1 \cdot \left(x_2^2+z_c^2\right)^2 + x_2 \cdot \left(x_1^2+z_c^2\right)^2}{\left(x_1^2+z_c^2\right)^2 + \left(x_2^2+z_c^2\right)^2} \end{aligned} \tag{12}$$

$$\begin{aligned} \Delta b &= x_b - x'_b \\ &= \frac{(x_3+x_4)}{2} - \frac{x_3 \cdot \left(x_4^2+z_c^2\right)^2 + x_4 \cdot \left(x_3^2+z_c^2\right)^2}{\left(x_3^2+z_c^2\right)^2 + \left(x_4^2+z_c^2\right)^2} \end{aligned} \tag{13}$$

When the offset is brought into the displacement subdivision algorithm (Eq. 2), the measured subdivision value after offset was shown in Eq. 14, expressed as

$$B' = \eta \cdot \frac{x_b - \Delta b}{\left(x_b - x_a\right) - (\Delta a + \Delta b)} \tag{14}$$

Therefore, when illumination distortion occurred, the error model generated by the IDM algorithm was Eq. 15, expressed as

$$E = B - B' = \eta \cdot \left[\frac{x_b}{x_b - x_a} - \frac{x_b - \Delta b}{\left(x_b - x_a\right) - (\Delta a + \Delta b)} \right] \tag{15}$$

When distortion existed, there was a certain offset in the IDM algorithm due to the change in illumination intensity, thus resulting in displacement measurement error (Eq. 15).

3.3. Error compensation algorithm

To realize compensation for light intensity, it was necessary to compensate the light intensity received by the linear image sensor. The method used here was to multiply the gray value of each pixel by a compensation value, so as to eliminate the centroid offset of coded lines caused by uneven illumination. According to the light intensity model, the compensation function should be inversely proportional to the distorted light intensity. Therefore, the compensation function was set, as shown in Eq. 16.

$$f(x) = \frac{x^2 + z_c^2}{z_c^2} \tag{16}$$

where x is the distance between any pixel position and the sensor's center point, $x^2+z_c{}^2$ the square of the optical path of light wave, and denominator $z_c{}^2$ used to realize normalization. After compensation, the light field intensity was expressed in Eq. 17 as

$$p'(x) = p(x) \cdot f(x) = k \cdot \frac{u_0^2}{z_c^2} = p(x)|_{x=0} \tag{17}$$

After the compensation operation, k, u_0, and z_c in Eq. 17 were seen to be constants. Illumination intensity at any position on the linear image sensor became the same as the gray value of the sensor center where $x = 0$ (according to Eq. 8, when $x = 0$, $p(0) = k \bullet u_0{}^2/z_c{}^2$). And the light intensity received within the range of the image sensor became uniform.

4. Simulation analysis

4.1. Simulation of line widths changing

According to the error model, when the widths of the two coding lines on both sides of the image center point were different, the error was large. It was assumed that the coded line between x_1 and x_2 was a "narrow" line with a width of η/M (Fig. 5), and the coded line between x_3 and x_4 a "wide" line with a width of $2\eta/M$ (M the variable to be simulated, with a larger M value indicating that the coding line became smaller).

To simulate the displacement measurement error, the variation range of x_a was set to $x_a = \{-\eta \sim 0\}$. As x_b-$x_a = \eta$, the value of the corresponding x_b was $x_b = x_a+\eta$. (When the circumference contained 2^N coded lines, η was the mapping value of $360^\circ/2^N$). Then, according to the variation of x_a and x_b, the values corresponding to x_1, x_2, x_3, and x_4 were respectively as follows:

The value of x_1 was x_a-$\eta/2M$,
x_2 was $x_a+\eta/2M$,
x_3 was x_b-η/M, and
x_4 was $x_b+\eta/M$.

To simulate the application environment, the height between the point light and grating disk was set to $h_1 = 4$ mm and the height between the image sensor and grating disk at $h_2 = 3$ mm. The transverse distance between the point light and linear image sensor was $d_c = 4$ mm. Through calculations, there were

$d_1 = d_c h_1/(h_1+h_2) = 2.2857$ mm,
$d_2 = d_c h_2/(h_1+h_2) = 1.7143$ mm,
$z_1 = (h_1{}^2+d_1{}^2)^{0.5} = 4.6070$ mm;
$z_2 = (h_2{}^2+d_2{}^2)^{0.5} = 3.4553$ mm, and

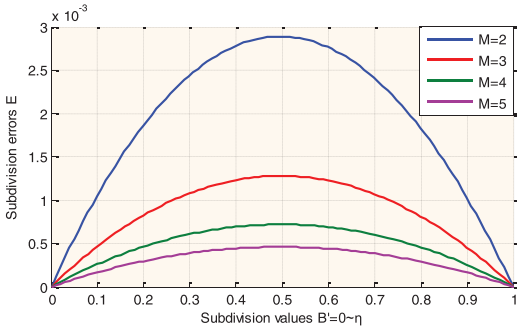

Fig. 6. Error curve when the width of coded line changed.

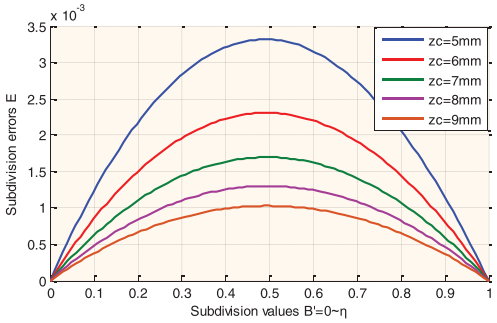

Fig. 7. Error curve when illumination distance changed.

$z_c = z_1 + z_2 = 8.0623$ mm.

When $M = 2$, 3, 4, and 5, B' was taken as the abscissa and $E = B\text{-}B$' as the ordinate. The curve of measurement error E was simulated according to Eq. 15 (Fig. 6).

In practical application, if $2^N = 512$ coded lines included in the circumference of grating disk, then η equivalent to mapping of angle value $360 \times 3600/512$ arcsec, at this time $\eta \approx 2531.25$ arcsec. Then, when $M = 2$, the error peak value was $E_{max} = 0.002887\eta = 7.31$ arcsec.

The abscissa in Fig. 6 represented the measurement value of displacement subdivision. At the position where the abscissa-axis was $B' = \eta/2$, the error reached the maximum. At positions $B' = 0$ and $B' = \eta$, the minimum error became $E = 0$. The ordinate in Fig. 6 represented the multiple of η, with the larger the η, the larger the error peak.

At the same time, the error peak was also seen to gradually decrease with increased M value. This was because, when the width of the coded line became narrow, the influence of illumination intensity distortion on the measurement gradually became smaller. However, to achieve a good reflection imaging effect, the value of M in practical application could not be infinitely larger.

Through simulation, it was concluded that:

1) The error peak decreased with decreased η. According to the preset of the grating disk, when 2^N coded lines were included in the circumference, the η was the mapping of $360°/2^N$. Therefore, the smaller the η was, the smaller the imaging area required by IDM. However, the optical system for reflection imaging did not include an imaging lens. Thus, to make full use of all the pixel range of the linear image sensor, the collected image needed to match the pixel range of the sensor. Thus, the value of η could not be arbitrarily reduced.
2) The error peak value decreased with increased M. A larger M meant that the width of the coded line became smaller. However, in reflection imaging, the narrow width of the coded line made the displacement measurement wrong. A too-narrow coded line did not achieve good reflection imaging. In general engineering application, the effect was better when $2< M <4$.

4.2. Simulation of illumination distance z_c changing

The displacement measurement error when the illumination distance z_c changed was simulated on the basis of Section 4.1, with the fixed value of M at 3. The optical distance from the point light to the image sensor central was assumed to be z_c = 5, 6, 7, 8, and 9 mm, with B' taken as the abscissa and $E = B\text{-}B$' as the ordinate, from which the curve of error $E = B\text{-}B$' was simulated (Fig. 7).

If 2^N=512 coded lines were included in the circumference of the grating disk in practical application, then η was equivalent to the mapping of the angle value $360 \times 3600/512$ arcsec, at this time $\eta \approx 2531.25$ arcsec. Then, when $z_c = 5$ mm, the error peak value was $E_{max} = 0.003318\eta = 8.4$ arcsec.

In the simulation curve, the peak value of error decreased gradually with change in illumination distance z_c. This was because, when the optical distance between the point light and linear image sensor became larger, the light intensity of the spherical wave became gradually similar to a plane wave and the distortion of the light intensity thus became smaller.

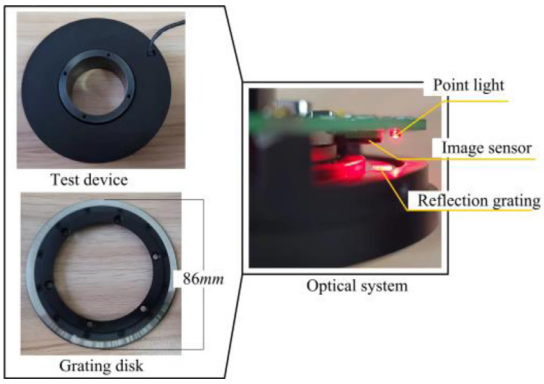

Fig. 8. Experimental device.

However, in practical application, the change of z_c produced two influences: 1) To increase the optical path distance of z_c, it was necessary to raise the height of h_1 or h_2, which made the volume of the measuring device larger and not conducive to miniaturization. 2) When the optical path z_c became larger, the light intensity reaching the linear image sensor also became weaker, which reduced the signal-to-noise ratio of the light wave signal and was not conducive to high-performance measurement. Thus, to ensure miniaturization design, z_c was ≤9 mm in the general design.

5. Experiments

5.1. Experimental device design

The performance of the proposed error compensation model was tested by designing a reflection-type IDM device based on the point light (Fig. 8).

The number of pixels in the employed linear image sensor was 1×256 pixels, sensor photosensitive length 13 mm, and pixel size 0.0508 mm. According to the preset, the wavelength of the point light used was 640 nm, point light height from the grating disk h_1 at 2.5 mm, height of the grating disk reached by the linear image sensor h_2 at 1.5 mm, and the transverse distance between the point light and linear image sensor d_c at 1.5 mm. After calculation, the optical path between the light and midpoint of the linear image sensor was

$z_1 = (h_1^2 + d_1^2)^{0.5} = 3.5355$ mm,

$z_2 = (h_2^2 + d_2^2)^{0.5} = 2.1213$ mm, and

$z_c = z_1 + z_2 = 5.6569$ mm.

It was calculated that $z_c^2 = (z_1 + z_2)^2 = 32$ mm^2. Therefore, the illumination compensation function was $f(x) = (z_c^2 + x^2)/z_c^2 = 1 + x^2/32$. The pixel number was set as i and, when the range of i was 1–256 pixels,

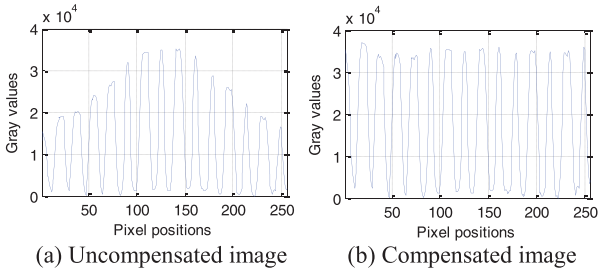

Fig. 9. Image comparison before and after compensation.

Table 1
Error value without compensation (Uint: arcsec).

No.	Errors	No.	Errors
1	0	10	9.1
2	6.3	11	4.1
3	−2.4	12	−7.4
4	5.8	13	−0.1
5	−5.6	14	9.6
6	−3.2	15	0.2
7	−5.1	16	5.9
8	−1.5	17	−3.4
9	−5.4		

the corresponding compensation function was Eq. 18, expressed as

$$f(i) = 1 + [(i - 128) \times 0.0508]^2/32 \tag{18}$$

The grating disk used in the experiment contains $2^N = 2^9 = 512$ coded lines in the circumference. The angle between adjacent coded lines was $360^\circ/512 = 0.7031^\circ$ and the mapping value forced to be $\eta = 2^{15}$, resulting in a measurement resolution of $360^\circ/2^{9+15}$ (24-bit). On the grating disk, M was preset at ≈3.2. At this time, the width range of coded line was

Variation range of x_1 was {-7.4η/6.4, -η/6.4}, x_2 at {-5.4η/6.4, η/6.4}, x_3 at {-η/3.2, 2.2η/3.2}, and x_4 at {η/3.2, 4.2η/3.2}.

5.2. Illumination compensation verification

The compensation effect of the compensation function was tested by examining the image collected by the image sensor (Fig. 6). When the compensation function was not added, the pattern collected by the linear image sensor is shown in Fig. 9a and the pattern collected after adding the compensation function $f(i)$ shown in Fig. 9b.

Before compensation, it was observed that there was clear "distortion" due to the influence of the spherical illumination intensity emitted by the point light (Fig. 9a). After adding compensation, the distortion in the "dark area" at the bottom of the gray value curve was significantly reduced (Fig. 9b). There was a slight "fluctuation" in gray values of the "bright area" at the top of the gray curve. Through analysis, these "slight fluctuations" were found to be caused by the uneven reflection intensity of the grating disk (caused by the different widths of the lines on the grating). At the same time, the accuracy of the compensation parameters z_1 and z_2 also affected the compensation effect. In practical application, these "fluctuations" could be ignored. Therefore, experiments demonstrated that the compensation function was effective.

5.3. Error comparison test

The performance of the proposed method was tested using a 17 polyhedron and laser autocollimator to examine the error. The test principle is shown in Fig. 11.

After error testing, the measured error data without compensation is shown in Table 1.

Table 2
Error value after compensation (Uint: arcsec).

No.	Errors	No.	Errors
1	0	10	21.3
2	8.5	11	8
3	−1.4	12	−3.4
4	14.1	13	3.4
5	5.6	14	16.3
6	−1.6	15	0.8
7	6.5	16	2.6
8	1.2	17	−0.8
9	−1.1		

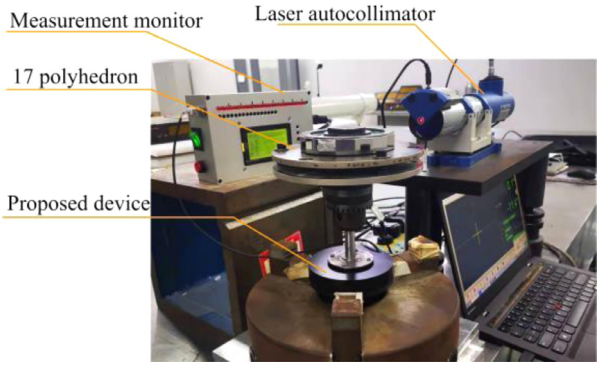

Fig. 10. Error test principle.

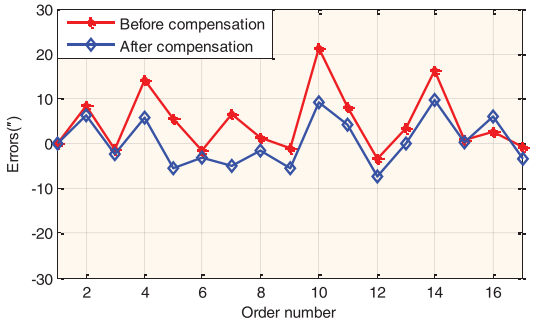

Fig. 11. Error comparison curve.

The standard deviation of the error data in Table 1 was $\sigma_1 = 5.4$ arcsec. Then, the compensation function was added to the experimental device and the error. Retested. The obtained error data is shown in Table 2.

The standard deviation of error data in Table 2 was $\sigma_2 = 7.03$ arcsec. For comparison, the error curves before and after compensation are shown in Fig. 12.

The fluctuations of the error curve after compensation were clearly reduced, compared to before compensation. The measurement accuracy was also improved from 7.03 arcsec to 5.4 arcsec. Thus, these experiments showed that the compensation was effective (Fig. 10).

6. Conclusions

IDM technology based on image recognition method has become a new high-performance displacement measurement technology in digital displacement feedback systems because of its high robustness, high fault tolerance, and high flexibility. In previous research, the transmission grating disk is illuminated by parallel light to realize pattern acquisition. Although it can achieve high performance measurement, it is limited by the volume of the parallel light. Thus, it cannot further realize miniaturization, which is required in application environments with limited volume.

To reduce the volume of the IDM device, a reflection-type displacement measurement method was proposed by irradiating the grating disk with a point light and then the error of this reflection-type IDM method analyzed. First, a reflective measuring light path was designed to be illuminated by a point light. Then, the measurement error model caused by point light illumination was established and a illumination intensity error compensation method proposed. Finally, the error compensation method was verified by experiments.

Through simulation of the proposed error model, it was concluded that: 1) Reducing the width of the coded line on the grating disk reduced the error caused by uneven illumination. 2) Increasing the height between the point light and grating disk reduced the measurement error. However, in practical engineering applications, the width of the coded line could not be arbitrarily reduced and the height of the point light not greatly improved. It was still necessary to compensate the error caused by uneven illumination.

Based on error analysis, an error compensation method was proposed. Experimental verification showed that measurement accuracy was improved from 7.5 to 4.5" using the proposed error compensation method on a grating disk with a diameter of 86 mm.

The error compensation method proposed was demonstrated to be effective. The study deeply analyzed the error factors when using a point light to realize reflection-type IDM and presented an effective error compensation method. This study provided a theoretical basis for miniaturized high-performance displacement measurement technology.

Declaration of Competing Interest

We declare that we have no financial and personal relationships with other people or organizations that can inappropriately influence our work, there is no professional or other personal interest of any nature or kind in any product, service and / or company that could be construed as influencing the position presented in, or the review of, the manuscript entitled “Error analysis and compensation method of displacement measurements based on reflection projection imaging”.

The authors declare no conflicts of interest.

Funding

This project is supported by the National Natural Science Foundation of China (Grant No. 52075520), Jilin Scientific and Technological Development Program (Grant No. 20210201097GX), and Youth Innovation Promotion Association of the Chinese Academy of Sciences (Grant No. 2022221).

References

[1] Anandan N, George B. A wide-range capacitive sensor for linear and angular displacement measurement. IEEE Trans Ind Electron 2017;64(7):5728–37.
[2] Yu Z, Peng K, Liu X, Chen Z, Huang Y. A high-precision absolute angular-displacement capacitive sensor using three-Stage time-grating in conjunction with a remodulation scheme. IEEE Trans Ind Electron 2019;66(9):7376–85.
[3] Chen Z, Pu H, Liu X, Peng D, Yu Z. A time-grating sensor for displacement measurement with long range and nanometer accuracy. IEEE Trans Instrum Meas 2015;64(11):3105–15.
[4] Park JW, Nguyen HX, Tran TN-C, Jeon JW. A linear compensation method for improving the accuracy of an absolute multipolar magnetic encoder. IEEE Access 2021;9:19127–38.
[5] Nguyen TH, Nguyen HX, Tran TN-C, Park JW, Le KM, Nguyen VQ, Jeon JW. An effective method to improve the accuracy of a vernier-type absolute magnetic encoder. IEEE Trans Ind Electron 2021;68(8):7330–40.
[6] Ye G, Liu H, Wang Y, Lei B, Shi Y, Yin L, Lu B. Ratiometric-linearization-based high–precision electronic interpolator for sinusoidal optical encoders. IEEE Trans Ind Electron 2018;65(10):8224–31.
[7] G. Ye, G. Zhao, H. Liu, B. Lu. Precise phase demodulation algorithm for sinusoidal encoders and resolvers, 2020, 67(10): 8778-8787.
[8] Yu H, Jia X, Q Wan, Liang L, Zhao C. High-resolution angular displacement technology based on varying Moiré figure phase positions. IEEE Sens J 2019;19(6):2126–32.
[9] Yu H, Wan Q, Lu X, Du Y, Liang L. High precision angular displacement measurement based on self-correcting error compensation of three image sensors. Appl Opt 2022;63(1):287–93.
[10] Das S, Sarkar TS. A new method of linear displacement measurement utilizing grayscale image. Int J Electron Electr Eng 2013;1(3):176–81.
[11] Bajić JS, Stupar DZ, Dakić BM, Živanov MB, Nagy LF. An absolute rotary position sensor based on cylindrical coordinate color space transformation. Sens Actuators A: Phys 2014;213:27–34.
[12] Dziwinski T. A novel approach of an absolute encoder coding pattern. IEEE Sens J 2015;15(1):397–401.
[13] Fu M, Zhang X. Study on the time-grating sensor method of the static light field type based on timing-driven. Mach Tool Hydraul 2015;43(24):75–9.
[14] Mu Y, Jiang J, Ding N, Ni Q, Chang Y. A 7.4 kHz, 20-bit image encoder with a CMOS linear image sensor. Opt Quant Electron 2019;51:321.
[15] Yuan P, Huang D, Lei Z, Xv C. An anti-spot, high-precision subdivision algorithm for linear CCD based single-track absolute encoder. Measurement 2019;137:143–54.
[16] Kim JA, Kim JW, Kang CS, Lee JY, Woo JH. Absolute planar position and full angle orientation sensor using a 2-D color-coded binary scale. IEEE Trans Instrum Meas 2020;69(5):2225–31.
[17] Yu H, Jia X, Wan Q, Zhao C, Sun Y. High-resolution angular measurement arithmetic based on pixel interpolations. Measurement 2020;149:106948.
[18] Yu H. Image-type displacement measurement resolution improvement without magnification imaging. Meas Sci Technol 2022;33:015103.
[19] Yu H, Wan Q, Lu X, Du Y, Liang L. High precision displacement measurement algorithm based on depth fusion of grating projection pattern. Appl Opt 2022;61(4):1049–56.
[20] Yu H, Wan Q, Zhao C, Han Q, Mu Z. Error compensation for low-density circular gratings based on linear image-type angular displacement measurements. IEEE Trans Ind Electron 2022 Early Access. doi:10.1109/TIE.2021.3139240.
[21] Yu H, Wan Q, Zhao C, Lu X, Sun Y. An anti-Stain algorithm of angular displacement base on single image sensor. Appl Opt 2020;59(7):1985–90.